A Rapid Genome-wide MicroRNA Screen Identifies *miR-14* as a Modulator of Hedgehog Signaling

Kevin Kim,[1,*] Arunachalam Vinayagam,[1] and Norbert Perrimon[1,2,*]
[1]Department of Genetics, Harvard Medical School, Boston, MA 02115, USA
[2]Howard Hughes Medical Institute, Harvard Medical School, Boston, MA 02115, USA
*Correspondence: kkim@genetics.med.harvard.edu (K.K.), perrimon@receptor.med.harvard.edu (N.P.)
 http://dx.doi.org/10.1016/j.celrep.2014.05.025

SUMMARY

MicroRNAs (miRNAs) are small noncoding RNAs that regulate gene expression by binding to sequences within the 3′ UTR of mRNAs. Because miRNAs bind to short sequences with partial complementarity, target identification is challenging. To complement the existing target prediction algorithms, we devised a systematic "reverse approach" screening platform that allows the empirical prediction of miRNA-target interactions. Using *Drosophila* cells, we screened the 3′ untranslated regions (3′ UTRs) of the Hedgehog pathway genes against a genome-wide miRNA library and identified both predicted and many nonpredicted miRNA-target interactions. We demonstrate that *miR-14* is essential for maintaining the proper level of Hedgehog signaling activity by regulating its physiological target, *hedgehog*. Furthermore, elevated levels of *miR-14* suppress Hedgehog signaling activity by cotargeting its apparent nonphysiological targets, *patched* and *smoothened*. Altogether, our systematic screening platform is a powerful approach to identifying both physiological and apparent nonphysiological targets of miRNAs, which are relevant in both normal and diseased tissues.

INTRODUCTION

MicroRNAs (miRNAs) are endogenously transcribed 19 to 25 nt small noncoding RNAs that posttranscriptionally regulate target mRNAs by pairing to complementary sequences, typically found in their 3′ UTRs, to repress mRNA translation, promote transcript decay or both (Bartel, 2009; Brodersen and Voinnet, 2009; Ghildiyal and Zamore, 2009; Hendrickson et al., 2009). In normal cells, multiple miRNAs cooperate to maintain a proper balance of various processes, including proliferation, differentiation, and cell death. In addition, individual miRNAs can regulate multiple mRNAs further complicating the gene regulatory networks of miRNAs. Therefore, dysregulation of miRNAs can have detrimental cellular consequences and has been associated with several human diseases ranging from metabolic and inflammatory disease to malignancy (Carè et al., 2007; Fiore et al., 2008;

Krützfeldt and Stoffel, 2006; Lu et al., 2005; Poy et al., 2004). According to the miR2Disease database (Jiang et al., 2009) that manually curates disease-associated miRNAs, both down- and upregulated miRNA dysregulation are equally prevalent.

Downregulation of miRNAs in diseased tissue can lead to aberrant expression of their target genes. Such genes are deemed "physiological targets" because their expression is tightly regulated by miRNAs in normal tissues. Conversely, upregulation of miRNAs in diseased tissue can further downregulate their physiological targets, preventing normal cell function. In addition, upregulated miRNAs are able to downregulate "apparent nonphysiological targets," which correspond to genes bearing miRNA binding sites that in the wild-type situation are unaffected. Therefore, identifying both physiological and apparent nonphysiological targets of miRNAs is essential for understanding the complex gene regulation by miRNAs in diseased tissues.

Target gene identification of miRNAs is challenging because they bind to their target mRNAs by partial complementarity over a short sequence and the rules of miRNA-mRNA interactions are not fully understood. Unlike the related siRNAs that require a perfect complementary match for cleavage of target mRNAs, miRNAs allow mismatches at positions 1, 9, or 10 relative to their 5′ end, whereas Watson-Crick pairing at positions 2–8, referred to as the "seed" region, is the minimal sequence required for silencing of their targets (Brennecke et al., 2005). In addition, despite the large number of target genes predicted to be affected by miRNA loss of function, individual miRNA knockouts lack strong phenotypic consequences. For example, in *C. elegans*, the majority of individual miRNA mutants display no major phenotype (Miska et al., 2007).

Use of miRNA target prediction algorithms has been valuable in identifying targets of many different miRNAs. However, these prediction algorithms are still not complete. Target prediction algorithms typically predict hundreds to thousands of target genes for an individual miRNA (Betel et al., 2010; Paraskevopoulou et al., 2013; Reczko et al., 2012; Ruby et al., 2007). However, most of these predicted genes may not correspond to true targets (Alexiou et al., 2009), and the algorithms often fail to identify validated miRNA targets (Johnson et al., 2005; Lal et al., 2009). Another complication is that predictions from several different algorithms generate lists of target genes with very little overlap, making decisions about which predictions to investigate difficult. Last, the majority of these predictions lack experimental validations.

Here, we devised a general "reverse approach" strategy for rapidly identifying targets of miRNAs whereby, rather than studying specific miRNAs, we screened the 3′ UTR of individual genes against miRNAs. Specifically, we screened the effect of 132 distinct miRNAs on the 3′ UTR of nine core components of the Hedgehog (Hh) signaling pathway, leading us to identify 59 miRNA-target interactions. The Hh pathway controls multiple developmental processes such as differentiation, pattern formation, and proliferation in various animals ranging from *Drosophila* to humans (Ingham et al., 2011; Jiang and Hui, 2008; McMahon et al., 2003). In addition, aberrant activation of Hh signaling in humans has been linked to growth and maintenance of various cancers (Barakat et al., 2010; Fan et al., 2004; Jiang and Hui, 2008; Kayed et al., 2004; Ruiz i Altaba, 1999; Taipale and Beachy, 2001; Watkins et al., 2003). We discuss how our experimentally based miRNA-target interactions approach compare to those obtained with the three most popularly used target prediction algorithms. Further, we focus on one miRNA, *miR-14*, that we find to regulate the 3′ UTRs of three Hh pathway components. In vivo analysis of *miR-14* targets shows how depending on its level of expression, a single miRNA targets different components of the same pathway and highlight the importance of identifying miRNA targets at different miRNA expression levels to fully understand loss or gain of function miRNA phenotypes.

RESULTS

Construction of miRNA Screening Platform for Screening Hh Pathway Components in Tissue Culture Cells

To facilitate the rapid identification of miRNAs that regulate core components of the Hh pathway, we used a firefly luciferase reporter to assay miRNA activity in *Drosophila* S2R⁺ cells. We constructed luciferase reporters for nine core components of the Hh pathway by cloning their 3′ UTR downstream of the firefly luciferase (Table S1). In addition, for the miRNA overexpression library, we used our previously generated collection of 95 constructs (Bejarano et al., 2012) that we complemented with an additional set of 33 constructs to increase the coverage of the collection (see Experimental Procedures). Because some plasmids cover multiple miRNAs, our miRNA overexpression library is composed of 128 overexpression plasmids covering 132 distinct miRNAs (see details in Table S2).

Next, to assess the activities of individual miRNAs, we cotransfected the luciferase 3′ UTR reporters with the miRNA overexpression plasmids into S2R⁺ cells. After 72 hr, the firefly luciferase levels were measured and normalized to the *Renilla* luciferase levels (Figure 1A). For each miRNA-target gene pair, we computed a negative log2 median fold change (LMF) score, where the higher LMF score corresponds to stronger repression of the target gene by the miRNA (Table S2).

Using the TargetScan (Ruby et al., 2007), DIANA (Paraskevopoulou et al., 2013; Reczko et al., 2012) and miRanda (Betel et al., 2010) target prediction databases, we compiled a list of miRNAs predicted to regulate the 3′ UTRs of Hh pathway components (Table S3). For each predicted miRNA-target pair, we extracted the confidence score assigned by individual tools. We only considered the miRNAs that are part of our screening

library and used the least stringent cutoff values for each tool to compile all possible miRNA-target predictions. Systematic comparison of the LMF score to the predicted confidence score reveals a weak but significant positive correlation (Figures 1B–1D). Furthermore, the median LMF scores increase as the number of prediction tools supporting the miRNA-target pair increases (Figure 1E). This suggests that the pairs with high LMF score are likely to be predicted by multiple target prediction tools as high-confidence miRNA-target pairs and demonstrate the reliability of the LMF scores.

Next, to systematically evaluate the performance of LMF scores, we created a positive reference set (PRS) and a random reference set (RRS). The PRS includes 24 miRNA-target pairs validated from the literature (six pairs) and complemented with high-confidence predictions (18 pairs). We constructed 1,000 RRS sets sampled from 736 nonspecific miRNA-target pairs (Table S4) (see Experimental Procedures). Analysis of true-positive rates (TPRs) and false-positive rates (FPRs) at various cutoff reveals robust performance of the LMF score (area under receiver operating characteristic [ROC] curve = 0.8). Furthermore, this analysis also facilitated the identification of appropriate cutoff value (LMF score ≥0.622) at which we achieved 33% TPR and 3% FPR (Figure 1F). Using this cutoff value, we generated a miRNA-target interaction network composed of 59 interactions connecting 43 miRNAs to nine Hh pathway members (Figure 1G). Strikingly, all nine Hh pathway 3′ UTR reporters responded to multiple miRNAs. Consistent with this result, computational analysis of miRNA target sites indicated that most genes bear binding sites of multiple miRNAs (Enright et al., 2003; Grün et al., 2005; Lewis et al., 2003; Maragkakis et al., 2011). Out of our 59 miRNA-target interactions, nine were supported by at least one of the three target-prediction algorithms, 16 were supported by two of the three target-prediction algorithms, and 11 were supported by all three (Figure 1H). In addition, we identified 23 miRNA-target interactions that were not predicted by any of the three target-prediction algorithms highlighting the limitation of the existing algorithms and the need for functional tests.

We identified 43 miRNAs that reduced the activity of the reporters and therefore constitute potential regulators of the Hh pathway. Of these, 30 miRNAs regulated a single Hh pathway component, whereas 13 miRNAs regulated multiple components. We selected *miR-14*, which was found to regulate both activators (*hh* and *smoothened* [*smo*]) and an inhibitor (*patched* [*ptc*]) of the Hh pathway (Figure 1G), for further characterization.

In Vitro Validations of *miR-14* Targets

We asked whether *miR-14* indeed targets *hh*, *ptc*, and *smo* by directly binding to its miRNA responsive elements (MREs) within their 3′ UTRs. To identify possible *miR-14* MREs in the 3′ UTR of each target gene, we used RNAhybrid (Rehmsmeier et al., 2004), a bioinformatics tool for finding the minimum free energy (mfe) hybridization sites for miRNAs. For each target gene, we selected the top candidate MREs based on their mfe scores and seed pairing rules and mutated the sequence complementary to the *miR-14* seed (Figure 2A). Mutating the potential MREs within the 3′ UTRs partially (*hh* and *smo*) and completely (*ptc*) relieved the suppression elicited by the addition of *miR-14* (Figure 2B). The partial rescue of the luciferase signals
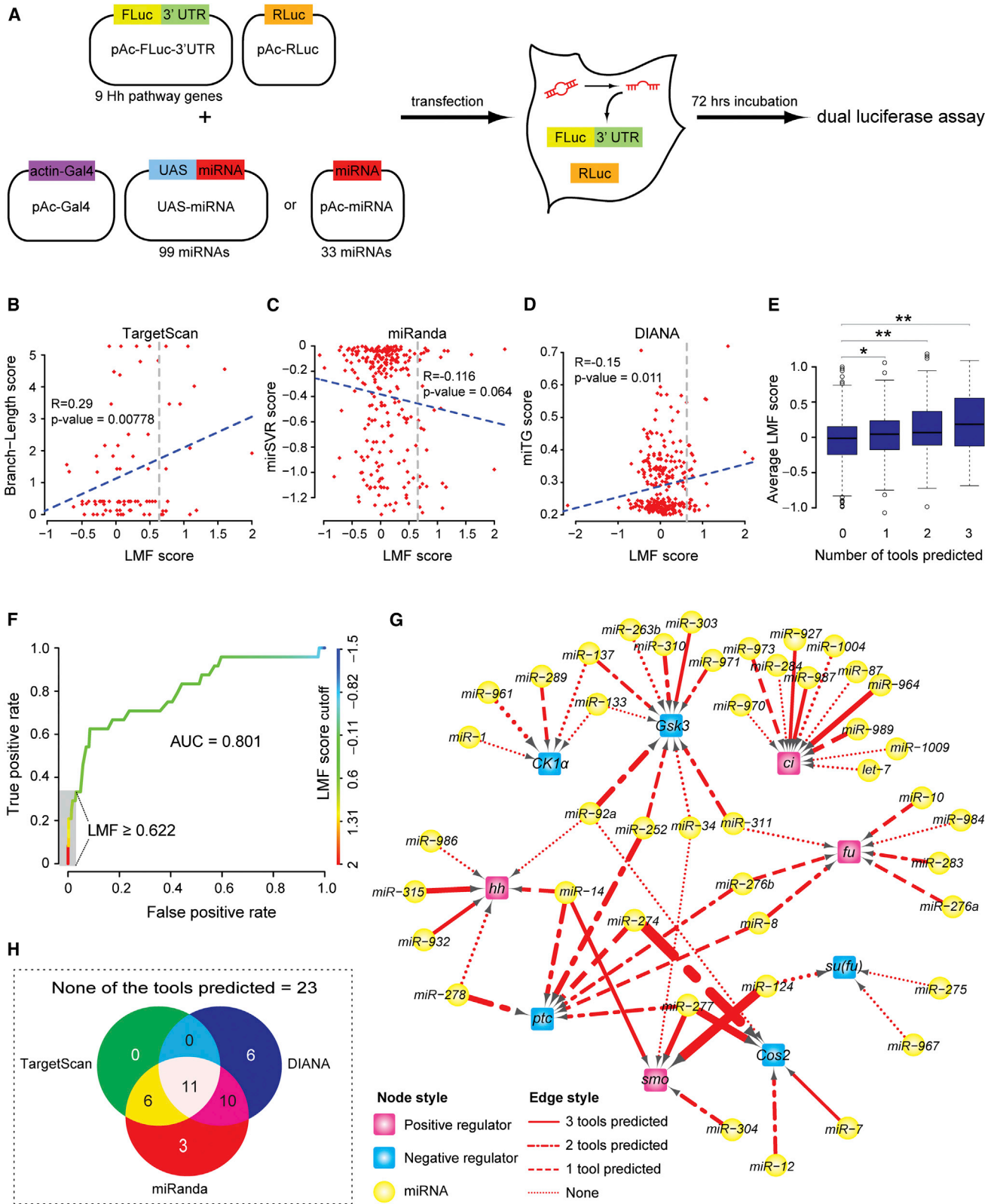
(legend on next page)
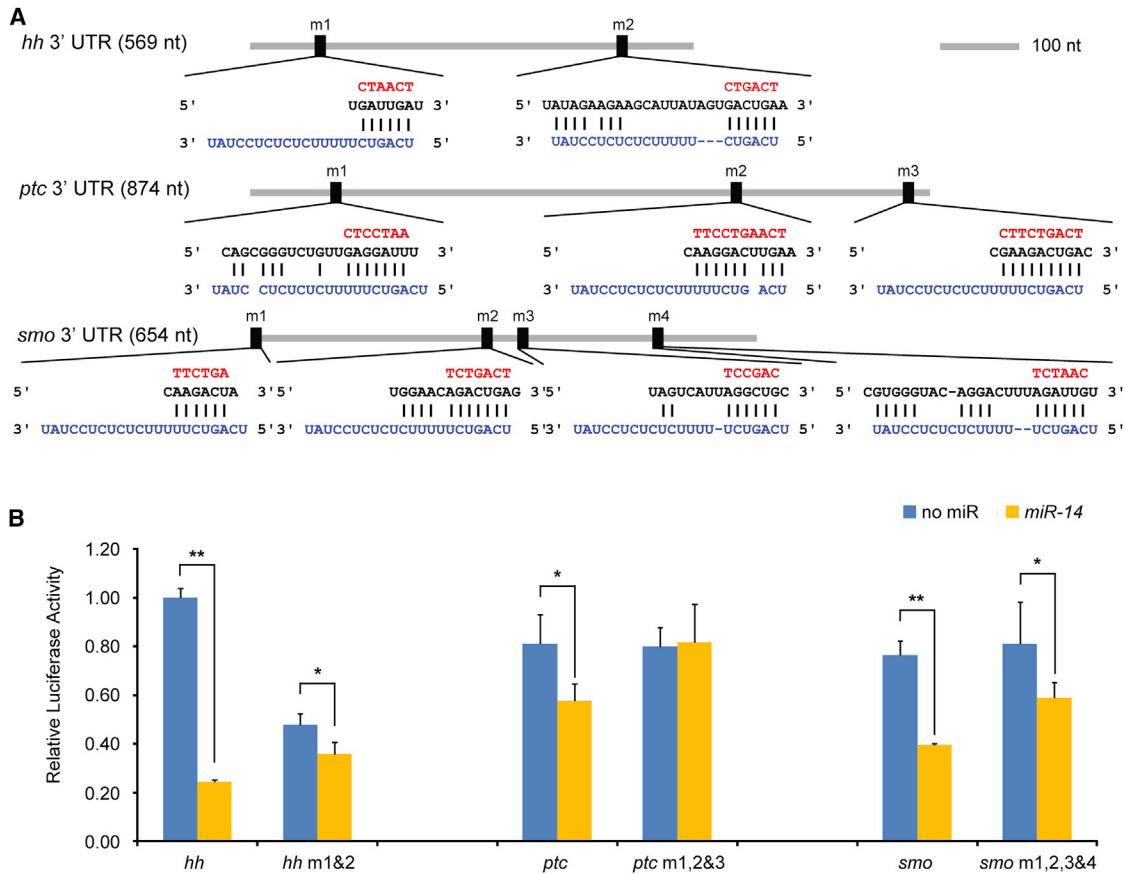
Figure 2. In Vitro Validations of *miR-14* Target Genes

(A) Potential *miR-14* binding sites within the 3′ UTRs of the three candidate target genes. All predicted binding sites were mutated as shown in red.

(B) Secondary luciferase reporter assay. *miR-14* was screened against wild-type and mutated 3′ UTRs to determine if the repressive activity of *miR-14* requires a direct interaction between *miR-14* and the predicted binding sites within the 3′ UTRs of the candidate target genes. Mutating the *miR-14* binding sites relieved repression. **p < 0.001 and *p < 0.05.

observed with the mutated MREs and *miR-14* is most likely due to additional, potentially still functional, *miR-14* MREs that were not mutated (Figures S1A–S1C). Collectively, these results demonstrate that direct interactions between *miR-14* and the MREs located within the 3′ UTR of the target genes are responsible for suppression of the luciferase signal.

Overexpression of *miR-14* Can Downregulate Endogenous Levels of Hh Signaling Pathway Genes

To determine whether *miR-14* affects Hh signaling in vivo, we focused on the *Drosophila* wing, where Hh regulates both tissue patterning and growth. Cells in the posterior (P) compartment of the developing wing disc express the secreted ligand Hh

Figure 1. Screen for miRNAs that Regulates Hh Signaling Pathway Components

(A) Outline of the primary screen. Genome-wide collection of 128 *Drosophila* miRNA overexpression plasmids that covers 132 distinct miRNAs were screened against the luciferase 3′ UTR reporters of nine core genes of the Hh pathway.

(B–D) Systematic comparison of the LMF scores from the entire screen to the predicted confidence scores from TargetScan, miRanda, and DIANA, respectively. Gray dashed lines mark the LMF score cutoff value (LMF score ≥0.622). Blue lines show the general correlation of the LMF score to the predicted confidence score from target prediction algorithms. Note that the confidence scores for miRanda (mirSVR score) increase as mirSVR scores decrease, thus the inverse in trend line. The significance of correlation is estimated using Pearson's product moment correlation coefficient (R).

(E) Comparison of the LMF scores to the miRNA-target pair predicted by number of tools. Box plots shows that the LMF score distributions of miRNA-target pairs predicted by single tool (1) two tools (2) and three tools (3) compared to the pairs that are not predicted by any of the tools (0). Wilcoxon test was used to test the significance of difference between two distributions. **p < 0.001 and *p < 0.05.

(F) Analysis of true-positive rates (TPR) and false-positive rates (FPR) at various LMF scores cutoffs. Gray box marks the cutoff value (LMF score ≥0.622) at which we achieved 33% TPR and 3% FPR. AUC, area under ROC curve.

(G) miRNA-target interaction network. The thickness of interaction lines indicates the range in LMF scores. The thickness in line increases as LMF scores increase.

(H) Venn diagram displaying the overlap of miRNA-target interaction predicted by individual prediction algorithms to the screen results.
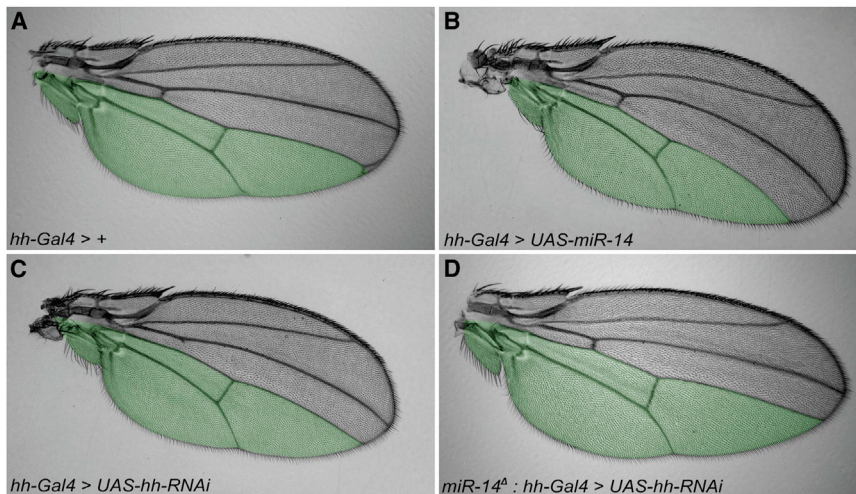
Figure 3. *miR-14* Can Modulate Wing Size by Regulating Hh Signaling

Area shaded in green (A–D) marks the region where *hh-Gal4* is active.

(A) Expression of *hh-Gal4* in the wild-type background.

(B) Overexpression of *miR-14* in the posterior compartment causes curvature of the wing.

(C) RNAi against *hh* in the posterior compartment phenocopies overexpression of *miR-14* suggesting that *miR-14* modulates Hh activity.

(D) Removal of endogenous *miR-14* restores the curved wing phenotypes observed in (C).

(E) Quantification of P compartment wing size and ratio of P compartment to the A compartment. Reduction of *hh* expression by RNAi and overexpression of *miR-14* significantly reduces the wing size of the P compartment. n = number of wings quantified. **p < 0.001 and *p < 0.05.
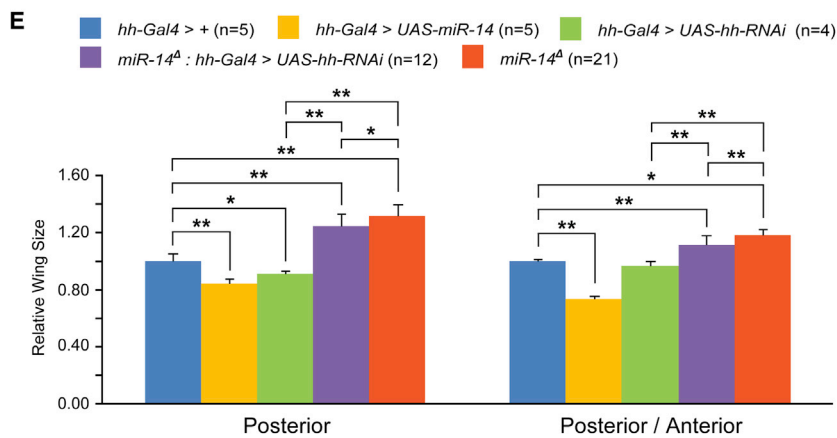
and induce *ptc* expression in the anterior (A) compartment to establish the A-P boundary. Expression of Hh and Smo is highest in the P compartment, whereas Ptc is exclusively expressed in the A compartment at the A-P boundary. Because the *hh*, *smo*, and *ptc* 3′ UTRs are sensitive to *miR-14* expression, we hypothesized that overexpressing *miR-14* in the compartments where these target genes are endogenously expressed should phenocopy their loss of function.

Reduction of Hh expression in the P compartment by RNAi significantly decreased wing size, evident by the slight curving of the wing toward the P compartment and by the quantification of wing size (Figures 3C and 3E). This phenotype is likely due to decreased Decapentaplegic (Dpp) signaling, a downstream target of the Hh signaling that regulates proliferation in both A and P compartments. Consequently, we also observed reduction in the A compartment, resulting in similar P/A compartment ratio to wild-type control (Figure 3E). Interestingly, overexpression of *miR-14* in the P compartment caused a significantly greater P compartment wing size defect (Figures 3B and 3E). One possibility is that, in addition to Hh, overexpression of *miR-14* in the P compartment represses factors that are required for Hh signaling. Alternatively, factors that are required for responding to Dpp signaling may also be target of *miR-14*. The wing size defect observed with loss of Hh expression by RNAi

was restored when endogenous *miR-14* was removed (Figure 3D), demonstrating that endogenous *miR-14* likely targets Hh and not Ptc and Smo because Ptc is not expressed in the P compartment, and, whereas Smo levels are highest in the P compartment, RNAi against *smo* in the P compartment does not alter the shape of the wing because Smo activity is mainly required at the A-P boundary and A compartment (Figure S2H) (Blair and Ralston, 1997). Interestingly, removal of endogenous *miR-14* in the presence of *hh*-RNAi significantly increased the overall size of the P compartment, further suggesting that additional targets of *miR-14* required for Hh and/or Dpp signaling may exist (Figure 3E). However, overall increase in the size of the P compartment was significantly less when compared to *miR-14* loss-of-function allele (Figure 3E), suggesting that regulation of Hh signaling by *miR-14* is partly to blame for the increase in overall wing size.

Ptc expression is highest at the A-P boundary and RNAi against *ptc* elevates Hh activity in that region resulting in an increased distance between the L3 and L4 wing veins (Figures S2D and S2′). Strikingly, overexpression of *miR-14* exhibited the opposite phenotype, decreasing the distance between the L3 and L4 veins, resembling instead decreased Hh signaling (Figures S2E–S2F′). One possible explanation is that because several rows of cells near the P compartment at the A-P boundary also express Smo, overexpression of *miR-14* in this region may inhibit both *ptc* and *smo*. Given that Ptc acts upstream of Smo, overexpression of *miR-14* will result in an overall decrease in Hh signaling activity. Consistent with this, overexpression of *miR-14*, as observed with *ptc*-RNAi, in the A-P region partially reduces the distance between the L3 and L4 veins (Figures S2G and S2G′), and RNAi against *smo* in the A-P boundary results in a clear decrease in the L3 and L4 intervein region (Figure S2I). In addition, overexpressing *miR-14* in the A compartment also
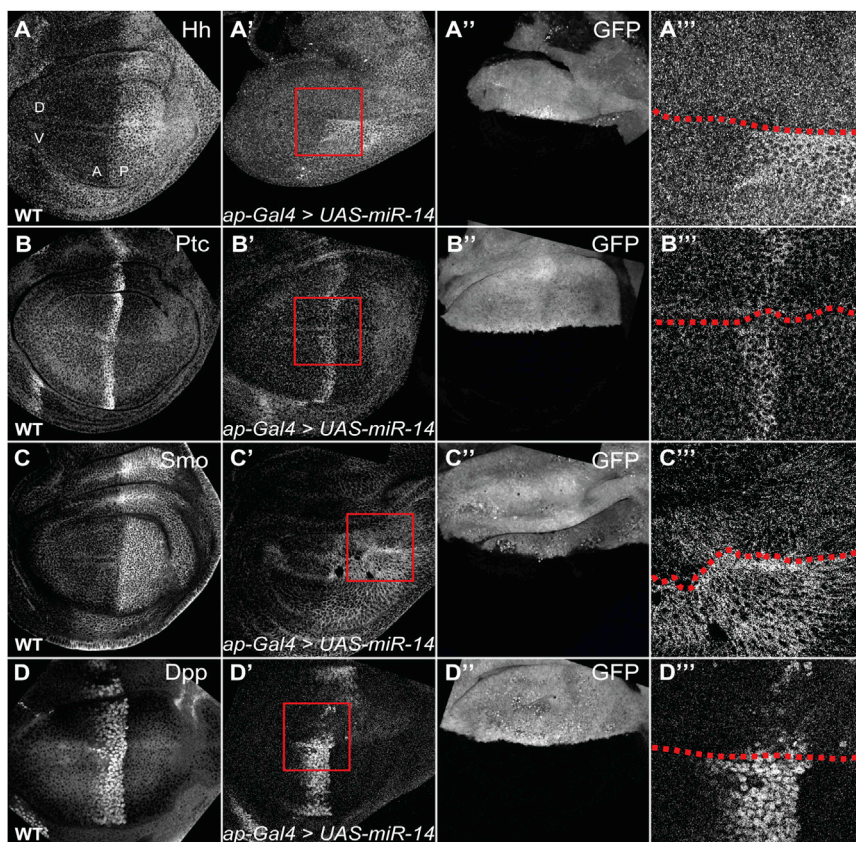
Figure 4. Overexpression of *miR-14* Reduces the Expression of Endogenous Hh Signaling Pathway Genes

(A–D′′′) Hh, Ptc, Smo, and Dpp-lacZ stainings in *Drosophila* third instar larva wing discs. Wing discs are oriented dorsal (D) up, ventral (V) down, anterior (A) left, and posterior (P) right. (A–D) Wild-type discs stained for Hh, Ptc, Smo, and Dpp-lacZ. (A′–D′) Expression of *miR-14* induced in the dorsal region of the wing disc using the *ap-Gal4* driver represses the expression of endogenous Hh, Ptc, and Smo and the Hh target gene, Dpp. (A′′–D′′) GFP expression marks the region where *ap-Gal4* is active and *miR-14* expression is induced. (A′′′–D′′′) Magnified view of the boxed area in (A′)–(D′). Red dotted lines mark the *ap-Gal4* boundary.

compared to Hh (Figures 4A–4A′′′ and 4C–4C′′′) and similar results were also observed with their respective sensors (Figure 2B). Collectively, our results suggest that overexpression of *miR-14* can suppress the expression of endogenous Hh, Ptc, and Smo at varying levels.

Because overexpression of *miR-14* can inhibit both positive (Hh and Smo) and negative (Ptc) regulators of the Hh pathway at varying levels, we analyzed the effect of *miR-14* overexpression on Hh pathway signaling output using Dpp expression as readout. Strikingly, Dpp expression was significantly reduced (Figures 4D–4D′′′), demonstrating that overexpression of *miR-14*, which can inhibit the endogenous expression of both positive and negative regulators of the Hh pathway, overall exerts a negative effect on Hh signaling activity when expressed at high levels.

Endogenous *miR-14* Regulates Hh Levels
Because overexpression of *miR-14* downregulates protein levels of endogenous Hh, Ptc, and Smo, we tested whether endogenous *miR-14* also represses these genes in vivo and therefore represent physiological targets. A previous study using a *miR-14* sensor has shown that *miR-14* is ubiquitously expressed throughout the entire wing disc and *miR-14* homozygous mutants are viable (Varghese et al., 2010). To determine whether *miR-14* mutants display any wing phenotypes suggestive of Hh signaling deregulation, we compared the adult wing area of *miR-14* mutant flies and found that *miR-14* mutant wings are ~18% larger than wild-type (Figures 5A and 5B). To test whether the increased wing size is due to elevated Hh activity, we reduced Hh level by RNAi in the *miR-14* mutant background. Reducing the amount of Hh activity in the mutants partially, but significantly, restored wing size (Figure 5B), suggesting that increased Hh signaling in *miR-14* mutants is at least in part responsible for the increased wing size.

Next, using a gain-of-function allele of *hh* called *Moonrat* (*hh^Mrt*), which primarily affects the anterior region of the wing (Felsenfeld and Kennison, 1995), we asked whether loss of

reduced the overall size of the A compartment causing the wing to curve in the anterior direction (Figure S2J). A likely model is that *miR-14* downregulates Smo levels in the A compartment, thus preventing activation of the Hh pathway and resulting in a smaller A compartment. In addition, overexpression of *miR-14* in the entire wing decreases the size of the wing (Figure S2C). These results collectively suggest that overexpression of *miR-14* in the wing leads to an overall reduction of Hh signaling.

To further evaluate the effect of *miR-14*, we examined directly the protein levels of endogenous Hh, Ptc, and Smo when *miR-14* was overexpressed. In wild-type wing discs, levels of Hh, Ptc, and Smo are identical in the dorsal (D) and ventral (V) compartments (Figures 4A–4C). However, when *miR-14* is overexpressed in the D compartment using *ap-Gal4*, the levels of Hh and Smo were significantly reduced (Figures 4A–4A′′′ and 4C–4C′′′), indicating that *miR-14* can suppress the expression of endogenous Hh and Smo. Interestingly, we observed little or no changes in the levels of Ptc (Figures 4B–4B′′′). One possible explanation is that because *ptc* is also a downstream target of Hh signaling, reducing the levels of Ptc by overexpressing *miR-14* will result in increased expression of *ptc*, which nullifies the repression by *miR-14*. Another possibility is that *miR-14* may weakly regulate Ptc in contrast to Hh and Smo. In fact, we observed similar results when all three 3′ UTR sensors were treated with *miR-14*. The *ptc* sensor was less sensitive to *miR-14* treatment compared to both the *hh* and *smo* sensors (Figure 2B). We favor the later explanation because the repression of Smo was also weaker when
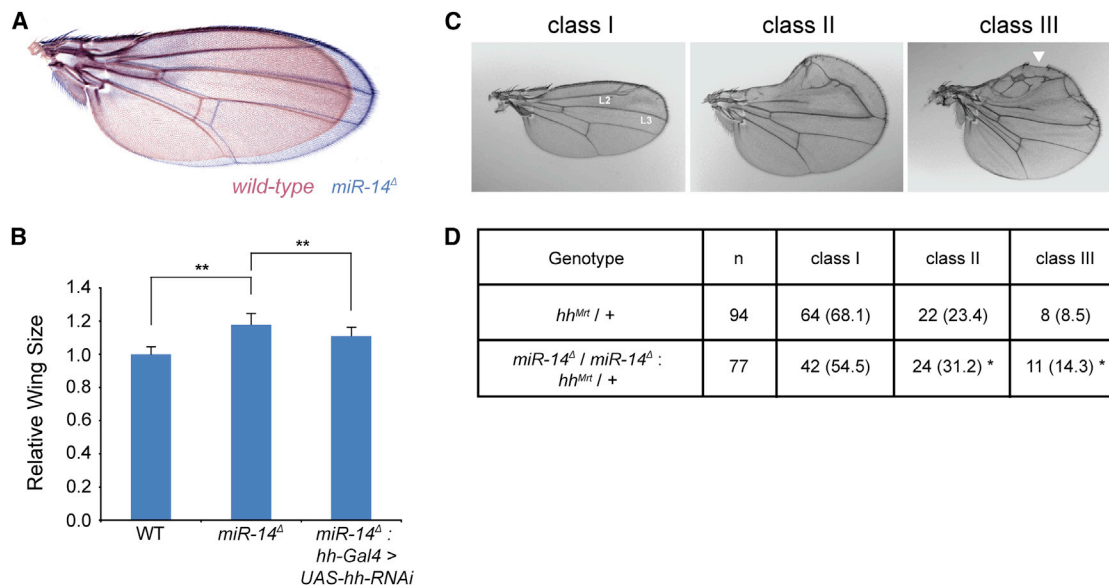
Figure 5. Endogenous *miR-14* Modulates Hh Expression

(A) Wild-type wing (blue) superimposed with *miR-14* mutant wing (magenta).

(B) Quantification of wing size from wild-type and *miR-14* mutants. Wing size defect is partially, but significantly restored when *hh* levels are reduced by RNAi. **p < 0.001.

(C) Severity of *hh^Mrt* wing phenotypes displayed in three classes, from mild to strong. Arrowhead marks the region where sensory bristles are missing. L2 and L3 mark the two major veins of the wing.

(D) Distribution of *hh^Mrt* wing phenotypes. "n" denotes the number of wings counted for each genotype; in parenthesis is the percentage of wings showing the phenotype. Absence of *miR-14* enhances both class II and III *hh^Mrt* phenotypes ($\chi^2 = 9.27$, *p < 0.01). Significance calculated using a chi-square test for comparing frequencies.

miR-14 could enhance the *Mrt* wing defects. For quantification purposes, we assigned mutant wing phenotypes to three different classes based on their severity. In class I *Mrt* phenotype, distal anterior region of the wing is slightly expanded with wing vein L2 partially duplicated. In class II, the distal anterior region of the wing is expanded and rounded. The L2 wing vein is frequently duplicated proximally and absent distally, whereas L3 vein is thickened distally. In class III, anterior compartment is almost completely rounded and all phenotypes observed in class II are present, but are more severe; often, both L2 and L3 veins are elaborately broadened. These are also associated with frequent loss of sensory bristles in the anterior region of the wing (Figure 5C). Removing both copies of *miR-14* partially, but significantly, enhanced the frequency of class II and III *Mrt* phenotypes (Figure 5D), suggesting that endogenous *miR-14* prevents further enhancement of the Hh activity of *hh^Mrt*.

miR-14 Ensures the Correct Number of Terminal Cells in the Tracheal System by Regulating Hh Activity

To determine whether *miR-14* can regulate Hh signaling in tissues other than the wing, we examined the *Drosophila* larval tracheal system where Hh signaling plays an important role in determining terminal cell fates (Glazer and Shilo, 2001). In the dorsal tracheal branch, which typically consists of five or six cells, one cell at the branch tip adopts the terminal cell fate marked by the expression of the serum response factor (SRF) (Guillemin et al., 1996). In addition, a second cell at the branch tip adopts a fusion cell fate and mediates fusion

of tracheal branches from the contralateral branches at the dorsal midline (Samakovlis et al., 1996a, 1996b). The two terminal cells from each side then branch extensively to deliver oxygen to neighboring tissues (Samakovlis et al., 1996a, 1996b) (Figure 6A).

Animals with excess levels of Hh signaling exhibit extra SRF-expressing cells that appear to arise from the branch cells located after the fusion cell (Glazer and Shilo, 2001). Because *miR-14* regulates the expression levels of Hh in the wing, we tested whether *miR-14* mutant larvae have defects in the number of terminal cells in the dorsal tracheal branches. Strikingly, *miR-14* mutant larvae possess extra SRF expressing cells (Figures 6B–6B''), and expression of *UAS-miR-14*, using the trachea-specific Gal4 driver, *btl-Gal4*, in *miR-14* mutant larvae, rescued the excess terminal cell phenotype (Figure 6C). Next, we tested whether the excess in terminal cells in *miR-14* mutant larvae results from an increase in Hh signaling activity. To reduce Hh activity, we either introduced the *hh* loss of function allele, *hh^AC*, or induced RNAi against *hh* in the *miR-14* mutant background and quantified the number of terminal cells. Strikingly, in both *hh^AC* heterozygotes and *hh*-RNAi animals, a reduction of excess terminal cells was observed in *miR-14* mutant larvae (Figure 6C), indicating that regulation of Hh signaling by *miR-14* is critical for determining the correct number of terminal cells. Collectively, our results from both the wing and the tracheal system indicate that *miR-14* regulates Hh signaling, a mechanism that may also extend to other tissues.
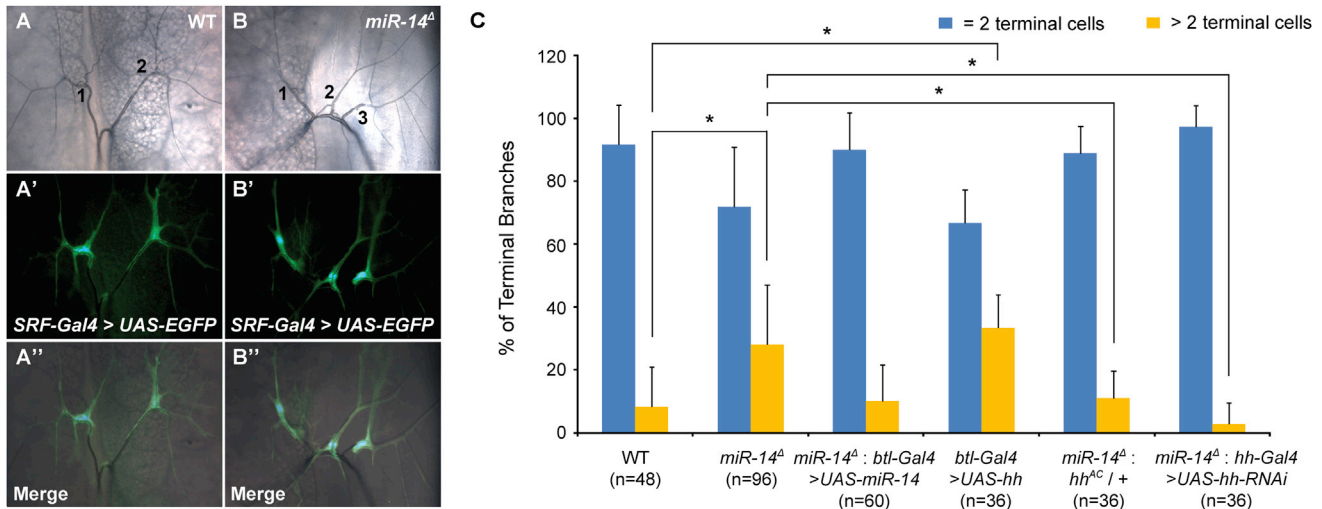
Figure 6. *miR-14* Regulates Hh Signaling in the Larval Tracheal System

(A) Dorsal branches of wild-type third instar larva trachea under bright field illumination.

(B) Dorsal branches of *miR-14* mutants. In wild-type, the two dorsal branches fuse and give rise to two terminal cells with multiple terminal branches, whereas *miR-14* mutants show excess terminal cells.

(A′ and B′) Terminal cells are marked using the terminal cell-specific Gal4 driver, *SRF-Gal4*, driving expression of EGFP.

(A″ and B″) Merged images of dorsal branches and labeled terminal cells.

(C) Quantitative analysis of terminal cell numbers in labeled genotypes. *miR-14* mutants exhibit more frequent instances of excess terminal cells, as observed when Hh is overexpressed (*btl-Gal4>UAS-hh*). Removing one functional allele of *hh* (*miR-14$^\Delta$: hh^{AC}/⁺*) or RNAi against *hh* (*miR-14$^\Delta$: hh-Gal4 / UAS-hh-RNAi*) in the *miR-14* mutant background restores the proper number of terminal cells. n, the number of dorsal branch pair examined. *$p < 0.05$.

hh Is a Physiological Target of Endogenous *miR-14*

To further investigate the regulation of target genes by endogenous *miR-14*, we measured the endogenous protein levels of Hh, Ptc, and Smo from whole pupae extracts. Hh levels were significantly elevated in *miR-14* mutants, whereas Ptc and Smo levels remained relatively unchanged (Figures 7A and 7B), suggesting that endogenous *miR-14* primarily functions to dampen Hh signaling by modulating Hh expression, but not Ptc or Smo.

Because miRNAs can also destabilize their target mRNAs, we checked the transcript levels of *hh*, *ptc*, and *smo* from total RNA of whole pupae. As expected, *hh* transcripts were elevated in *miR-14* mutants (Figure 7C). Interestingly, *ptc* mRNAs increased by nearly 3-fold in the mutants whereas *smo* levels were increased by 2-fold (Figure 7C). Because *ptc* is also a direct target of the Hh pathway, one possibility is that increased Hh signaling activity in *miR-14* mutants caused an increase in *ptc* transcript levels. Although it is unclear why an increase in *ptc* and *smo* transcript levels do not translate into more protein levels in *miR-14* mutants, an alternative mechanism regulating Ptc and Smo proteins production in *miR-14* mutants may exist. Alternatively, increase in both *ptc* and *smo* transcript levels might be an indirect effect of removing endogenous *miR-14*. It is possible, given the ability of miRNAs to regulate many different processes, that *miR-14* indirectly regulates the expression of *ptc* and *smo*.

We also measured the expression levels of Hh target genes, *wg* and *dpp*, and found that both genes were increased in the *miR-14* mutants (Figure 7C). To investigate whether increase in *wg* and *dpp* levels leads to hyperactivation of the Wg and Dpp signaling pathways, we examined the expression levels of the Wg target gene, *senseless*, and Dpp target genes, *spalt* and

omb. As expected, the levels of all three target genes were elevated in the *miR-14* mutant (Figure 7C). Although it is possible that all three genes are also physiological targets of *miR-14*, it is most likely an indirect result of increased Hh signaling in the *miR-14* mutant because both Wg and Dpp pathways are downstream of Hh signaling. These results collectively show that endogenous *miR-14* maintains the proper balance of Hh signaling activity by primarily regulating Hh expression, a physiological target, but not Ptc and Smo, supporting the model that they likely represent apparent nonphysiological targets (Figure 7D).

DISCUSSION

Previous miRNA gain-of-function studies using specific phenotypes and pathway sensors as readouts generated many interesting phenotypes and identified several candidate miRNAs in specific signaling pathways (Bejarano et al., 2012; Silver et al., 2007; Szuplewski et al., 2012). However, these approaches faced difficulties in identifying biologically significant targets. Here, we designed a fast and efficient approach to identify miRNA targets, whereby rather than studying the function of individual miRNAs, we screen for all possible targets of all miRNAs in a given signaling pathway. This study uses a genome-wide collection of *Drosophila* miRNAs to screen for potential target genes among specific components of a signaling pathway. Using luciferase as readout, we were able to quickly and easily measure the effect that different miRNAs have on the genes being interrogated. This systematic miRNA screening platform can be used to elucidate miRNA-target relationships for genes in various other processes.
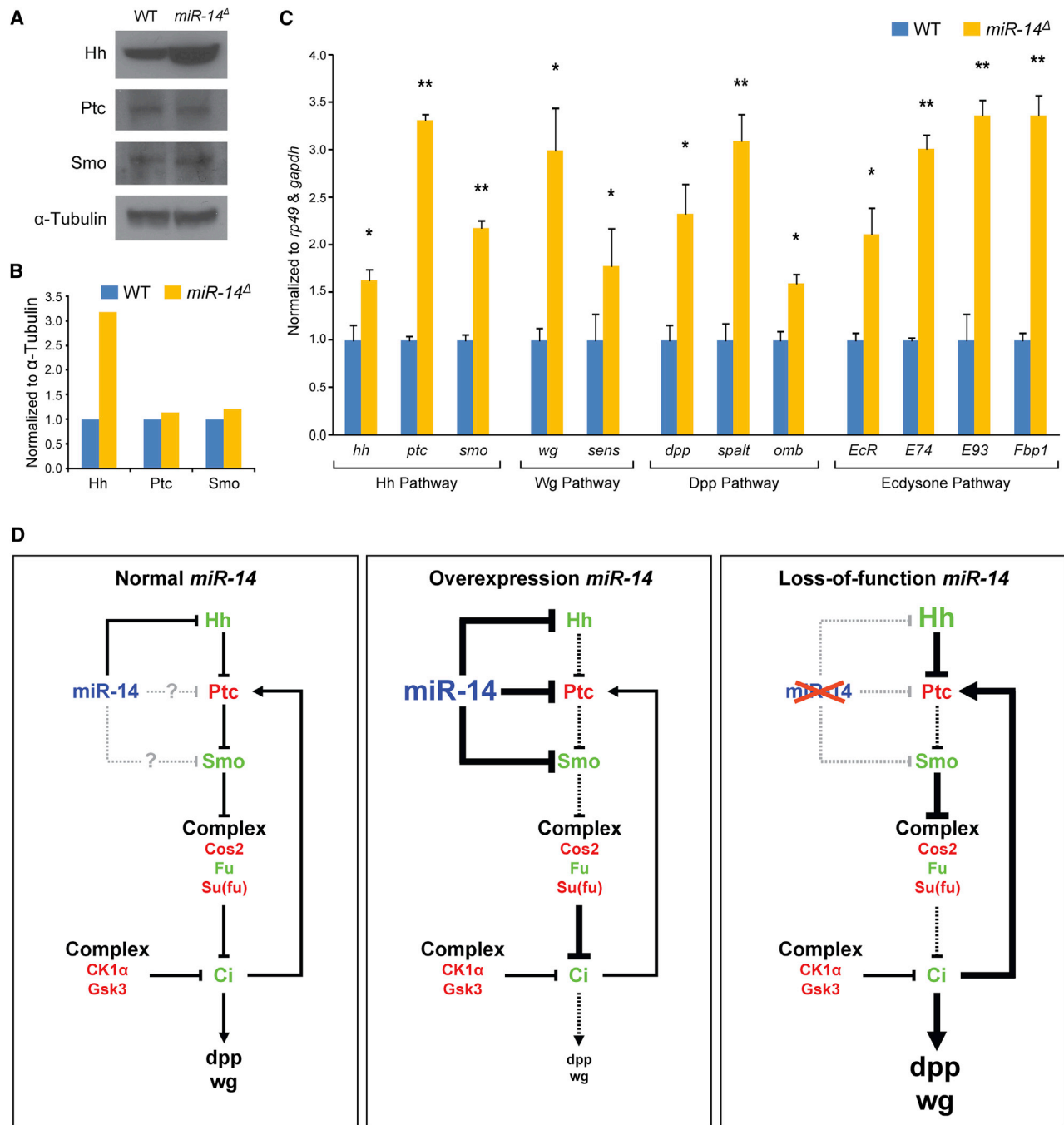
Figure 7. Hh Is a Physiological Target of *miR-14*

(A) Western blot analysis of *miR-14* mutant pupae. Absence of *miR-14* results in elevated Hh protein levels, whereas Ptc and Smo levels remain relatively unaffected. α-Tubulin was used as loading control.

(B) Quantitative analysis of the western blot from (A).

(C) Quantitative PCR analysis from *miR-14* mutant pupae. Levels of three Hh pathway genes *hh*, *ptc*, and *smo* are upregulated in *miR-14* mutants. Target genes of Hh signaling *wg* and *dpp*, and their respective target genes are also upregulated in *miR-14* mutant pupae. Levels of *EcR*, a validated target of *miR-14*, and its downstream target genes, *E74*, *E93*, and *Fbp1*, are elevated. **$p < 0.001$ and *$p < 0.05$.

(D) Model showing regulation of *hh* signaling pathway by *miR-14*. Genes labeled in green or red represent predominantly positive or negative regulators of the pathway, respectively. (Left) During normal development, *miR-14* regulates Hh signaling by buffering Hh levels. Physiological regulation of both Ptc and Smo might also exist, yet no such evidence has been identified in our current work. (Middle) Overexpression of *miR-14* results in strong repression of Hh as well as its apparent nonphysiological targets, Ptc and Smo, resulting in decreased Hh signaling. (Right) In the absence of *miR-14*, Hh levels increase resulting in increased Hh signaling.

Systematic performance evaluation of the LMF scores by analyzing the TPR and FPR allowed us to identify an appropriate cutoff value at which we achieved 33% TPR and 3% FPR. Our cutoff was stringent enough that previously identified interactions between *miR-12* and *Costal-2* (*Cos2*) and *miR-283* and *Fu* were included, but interactions with *smo* were excluded (Friggi-Grelin et al., 2008). Evaluation of our screen results to three of the popularly used prediction algorithms demonstrated that there is a positive correlation between the LMF scores and the number of miRNA-target predictions made. Furthermore, our screen revealed 23 miRNA-target interactions, representing ~39% of the total miRNA-target interactions. Interestingly, the *miR-14-hh* interaction was predicted by only one prediction algorithm, whereas *miR-14-ptc* and *miR-14-smo* interactions were identified by multiple algorithms. Furthermore, *miR-14-hh* interaction was only predicted when the least stringent cutoff value was used. The miRNA target gene (miTG) score assigned by DIANA for *miR-14-hh* is 0.212, which is much lower than the high-confidence miTG score of ≥ 0.5. This result further highlights the limitation of the existing algorithms and the need for functional tests.

We identified and characterized in detail *miR-14* that can regulate three components of the Hh pathway, *hh*, *ptc*, and *smo*. We have shown that *miR-14* overexpression can decrease the levels of all three proteins at varying levels and cause an overall decrease in Hh signaling as evidenced by the reduction of Dpp expression in the wing imaginal discs and by the adult wing outgrowth. We have also presented evidence that this regulation is mediated through the direct binding of *miR-14* seed sequences to the *miR-14* MREs located within the 3′ UTRs of all three genes. We have also presented data demonstrating that *hh* is a physiological target of *miR-14*, whereas *ptc* and *smo* appear to be nonphysiological targets. However, there are several alternative explanations that might impede us from categorizing both *ptc* and *smo* as physiological targets. For example, regulation of Ptc and Smo by *miR-14* may be very weak and not detectable by western blot analysis. In fact, the effect of an individual miRNA on a protein target level tends to be subtle, usually less than 2-fold (Baek et al., 2008). In support of this explanation, the amount of repression elicited by *miR-14* on both *ptc* and *smo* 3′ UTR sensors and Ptc and Smo levels in the wing discs are far less robust compared to Hh. Alternatively, additional miRNAs may act in a combinatorial manner and downregulate Ptc and Smo even in the absence of *miR-14*. In fact, our screen identified several other miRNAs that can also reduce the *ptc* and *smo* sensor levels. Finally, because Hh negatively regulates Ptc levels, derepression of Ptc in *miR-14* mutants maybe nullified by the increased levels of Hh.

Although *miR-14* is well conserved in distantly related *Drosophila* species, it is missing in vertebrates such as Zebrafish and humans. Nevertheless, regulation of Hh signaling by miRNAs seems to be conserved across diverse species. For example, *Suppressor of fused* (*Su(fu)*) is targeted by *miR-214* in Zebrafish to enable precise specification of muscle cell types by sharpening cellular responses to Hh (Flynt et al., 2007). In non-small-cell lung cancer cell line, *miR-212* acts as oncogene by targeting PTCH1, human homolog of *Drosophila* Ptc, to increase cell proliferation, migration, and invasion (Li et al., 2012),

whereas in chronic myeloid leukemia (CML), *miR-326* targets Smo to decrease cell proliferation and increase apoptosis (Babashah et al., 2013).

Although, *ptc* and *smo* seem to be apparent nonphysiological targets of *miR-14*, this information is valuable because dysregulation of miRNAs are common features of many diseases. In addition, given that miRNA replacement therapies are currently being tested as possible treatments for various diseases, information regarding apparent nonphysiological targets becomes very important to prevent unnecessary side effects. Therefore, considering the importance of identifying both physiological and apparent nonphysiological targets, we propose that our fast and efficient approach of identifying miRNA targets can help understand the complex gene regulatory network of miRNAs.

EXPERIMENTAL PROCEDURES

DNA Constructs and Cloning

Reporter plasmids were constructed by cloning firefly luciferase into the KpnI/EcoRI site of pAc5.1/V5-His C (Invitrogen). Next, the 3′ UTR of each target gene was cloned into the EcoRI/SacI site, with the exception of *Fu* that was cloned into the NheI/SacI site. The 3′ UTR for individual genes was cloned based on annotated sequences provided by Flybase (http://www.flybase.org). A complete list of 3′ UTR primers can be found in Table S1.

Most miRNA overexpression plasmids used to prepare the screening platform have been previously described (*UAS-dsRed-miRNA* collection described in Bejarano et al., 2012). To expand coverage, we prepared 33 additional miRNAs overexpression plasmids by amplifying ~400–700 nt fragments encompassing miRNA genes from genomic DNA and cloned them into pAc5.1/V5-His C. Altogether, the resource comprises 128 miRNA overexpression plasmids that covers 132 distinct miRNAs (Table S2). Note that we chose to clone the new miRNAs into a vector under the control of constitutively active *Actin* promoter rather than UAS to minimize the number of plasmids needed for transfection. Prior to constructing the additional miRNA constructs, we compared the knockdown efficiency of *senseless* 3′ UTR reporter, which has been previously shown to be regulated by *miR-9a* (Li et al., 2006), using both pAc and UAS vectors. Both *pAc-miR-9a* and *UAS-dsRed-miR-9a* overexpression plasmids were equally effective at reducing the luciferase level of *senseless* 3′ UTR reporter (Figure S3).

A complete list of miRNAs can be found in Table S2. Primer sequences will be provided upon request. The screening platform will be publicly available at the *Drosophila* RNAi Screening Center (DRSC).

To mutate the seed sequence of *miR-14* and potential MREs in the 3′ UTRs of target genes, we followed the instructions of QuikChange II XL Site-Directed Mutagenesis Kit (Stratagene).

Luciferase Reporter Assay

Drosophila S2R⁺ cells were maintained in Schneider's *Drosophila* Medium (Gibco) with 10% heat-inactivated FBS (Sigma) and 1% Pen/Strep (Gibco) at 25°C. Experiments were performed in 96-well plates excluding the outer wells. The wells were seeded with 20 ng of plasmid expressing *pAc-miRNAs* or 20 ng of plasmid expressing *UAS-dsRed-miRNAs* and 5 ng of *Actin-Gal4* plasmid prior to the start of the experiment. Each well was transfected with 5 ng of firefly luciferase reporter plasmid and 5 ng of *Renilla* luciferase reporter plasmid for transfection control. Transfection was performed using Effectene Transfection Reagent (QIAGEN). After 72 hr, luciferase activities were measured using DualGlo (Promega).

Computing miRNA-Target Interaction Score

We computed the normalized fold change value *x* for the given miRNA *i* and 3′ UTR region of gene *j* as follows:

$$x_{ij} = \frac{(S_{ij}/(U_j/C))}{(M_i/C)},$$

where S_{ij} is normalized firefly signal (ratio of firefly/Renilla luciferase levels) from the tested pair of miRNA i and 3′ UTR of gene j, U_j is signal from 3′ UTR control (lacking miRNA) and M_i is signal from miRNA control (lacking 3′ UTR). C is the signal from control without both 3′ UTR and miRNA. Next, we computed the median of fold change values ($\bar{x}$) from the three replicates. The negative log2 median LMF is computed as:

$$LMF_{ij} = -\log2(\bar{x}_{ij}).$$

Integrative Analysis with a Predicted miRNA-Target Network

To compare the LMF score with predicted miRNA target, we collected the potential miRNAs that could regulate the Hh pathway members from TargetScan (http://www.targetscan.org/) (Ruby et al., 2007), miRanda (http://www.microrna.org/microrna/home.do) (Betel et al., 2010), and DIANA (http://diana.cslab.ece.ntua.gr/) (Paraskevopoulou et al., 2013; Reczko et al., 2012) databases. For all three databases, least cutoff values were used to extract all possible miRNA-target relations and each extracted pair was associated with respective scores assigned by the tools (Branch-Length score for TargetScan, miRNA Support Vector Regression (mirSVR) score for miRanda and miTG score for DIANA). The trend line was fitted using the linear regression model (*LMF* ∼Prediction score) implemented in R (http://www.r-project.org/). All the integrative analyses were performed using in-house developed perl scripts.

Validation of LMF Score Performance

In order to choose the LMF cutoff value, we created a positive reference set (PRS) and a random reference set (RRS). The PRS includes 24 miRNA-target gene (member of Hh pathway) interactions curated from literature (six pairs) and high-confidence predictions (18 pairs) that overlap with our screening space. High-confidence miRNA-target interactions refer to the pairs that are predicted by two or more independent tools as high-confidence interactions (TargetScan: branch-length score ≥ 0.8; miRanda: mirSVR score ≤ -0.5; DIANA: miTG score ≥ 0.5). To construct RRS, we first compiled a list of 736 potential noninteracting pairs from the screening space (1,160 possible pairs) that are not overlapping with PRS and not predicted as miRNA target by any of the tools even with the least stringency cutoff. From this potential noninteracting pairs, we randomly sampled 1,000 RRS sets (size of each RRS is equal to the size of PRS). We analyzed the true-positive rate (TPR) and false-positive rate (FPR) values for various *LMF* score cutoff values. For a given *LMF* score cutoff value i, the TPR and FPR are computed as follows:

$$TPR_i = \frac{TP_i}{(TP_i + FN_i)}$$

$$FPR_i = \frac{FP_i}{(FP_i + TN_i)}$$

$$i \in \{LMF | -1.5 \leq LMF \leq 2\}.$$

TP_i, FN_i, FP_i, and TN_i correspond to true-positive, false-negative, false-positive, and true-negative values at given *LMF* cutoff value i, respectively. The Hh miRNA-target network was constructed using at chosen cutoff value (LMF $\geq$ 0.62). The network is visualized with Cytoscape software (http://www.cytoscape.org/).

Immunostaining, Confocal Imaging, and Analysis

Immunostainings of larval wing imaginal discs were performed as previously described (Belenkaya et al., 2004). Primary antibodies were mouse anti-Ptc (1:40; DSHB, Apa-1), mouse anti-Smo (1:50; DSHB, 20C6), rabbit anti-Hh (1:50; kindly provided by Dr. Xinhua Lin), and rabbit anti-β-Gal (1:1000; Cappel). Primary antibodies were detected by anti-mouse or anti-rabbit secondary antibodies conjugated to Alexa-Fluor 594 and 647 (1:1,000; Invitrogen). Fluorescent images were acquired with a Leica TCS SP2 AOBS. Images were processed using Adobe Photoshop.

Tracheal Terminal Branch Imaging and Analysis

Third instar larvae were heat killed (70°C for 10–15 s), mounted in 50% glycerol and examined under a Zeiss Axioskop 2 compound fluorescence microscope. Average values and their corresponding SDs were calculated, and t test analysis was performed with Microsoft Excel.

REFERENCES

Alexiou, P., Maragkakis, M., Papadopoulos, G.L., Reczko, M., and Hatzigeorgiou, A.G. (2009). Lost in translation: an assessment and perspective for computational microRNA target identification. Bioinformatics *25*, 3049–3055.

Babashah, S., Sadeghizadeh, M., Hajifathali, A., Tavirani, M.R., Zomorod, M.S., Ghadiani, M., and Soleimani, M. (2013). Targeting of the signal transducer Smo links microRNA-326 to the oncogenic Hedgehog pathway in CD34 CML stem/progenitor cells. Int J Cancer.

Baek, D., Villén, J., Shin, C., Camargo, F.D., Gygi, S.P., and Bartel, D.P. (2008). The impact of microRNAs on protein output. Nature *455*, 64–71.

Barakat, M.T., Humke, E.W., and Scott, M.P. (2010). Learning from Jekyll to control Hyde: Hedgehog signaling in development and cancer. Trends Mol. Med. *16*, 337–348.

Bartel, D.P. (2009). MicroRNAs: target recognition and regulatory functions. Cell *136*, 215–233.

Bejarano, F., Bortolamiol-Becet, D., Dai, Q., Sun, K., Saj, A., Chou, Y.T., Raleigh, D.R., Kim, K., Ni, J.Q., Duan, H., et al. (2012). A genome-wide transgenic resource for conditional expression of Drosophila microRNAs. Development *139*, 2821–2831.

Belenkaya, T.Y., Han, C., Yan, D., Opoka, R.J., Khodoun, M., Liu, H., and Lin, X. (2004). Drosophila Dpp morphogen movement is independent of dynamin-mediated endocytosis but regulated by the glypican members of heparan sulfate proteoglycans. Cell *119*, 231–244.

Betel, D., Koppal, A., Agius, P., Sander, C., and Leslie, C. (2010). Comprehensive modeling of microRNA targets predicts functional non-conserved and non-canonical sites. Genome Biol. *11*, R90.

Blair, S.S., and Ralston, A. (1997). Smoothened-mediated Hedgehog signalling is required for the maintenance of the anterior-posterior lineage restriction in the developing wing of Drosophila. Development *124*, 4053–4063.

Brennecke, J., Stark, A., Russell, R.B., and Cohen, S.M. (2005). Principles of microRNA-target recognition. PLoS Biol. *3*, e85.

Brodersen, P., and Voinnet, O. (2009). Revisiting the principles of microRNA target recognition and mode of action. Nat. Rev. Mol. Cell Biol. *10*, 141–148.

Carè, A., Catalucci, D., Felicetti, F., Bonci, D., Addario, A., Gallo, P., Bang, M.L., Segnalini, P., Gu, Y., Dalton, N.D., et al. (2007). MicroRNA-133 controls cardiac hypertrophy. Nat. Med. 13, 613–618.

Enright, A.J., John, B., Gaul, U., Tuschl, T., Sander, C., and Marks, D.S. (2003). MicroRNA targets in Drosophila. Genome Biol. 5, R1.

Fan, L., Pepicelli, C.V., Dibble, C.C., Catbagan, W., Zarycki, J.L., Laciak, R., Gipp, J., Shaw, A., Lamm, M.L., Munoz, A., et al. (2004). Hedgehog signaling promotes prostate xenograft tumor growth. Endocrinology 145, 3961–3970.

Felsenfeld, A.L., and Kennison, J.A. (1995). Positional signaling by hedgehog in Drosophila imaginal disc development. Development 121, 1–10.

Fiore, R., Siegel, G., and Schratt, G. (2008). MicroRNA function in neuronal development, plasticity and disease. Biochim. Biophys. Acta 1779, 471–478.

Flynt, A.S., Li, N., Thatcher, E.J., Solnica-Krezel, L., and Patton, J.G. (2007). Zebrafish miR-214 modulates Hedgehog signaling to specify muscle cell fate. Nat. Genet. 39, 259–263.

Friggi-Grelin, F., Lavenant-Staccini, L., and Therond, P. (2008). Control of antagonistic components of the hedgehog signaling pathway by microRNAs in Drosophila. Genetics 179, 429–439.

Ghildiyal, M., and Zamore, P.D. (2009). Small silencing RNAs: an expanding universe. Nat. Rev. Genet. 10, 94–108.

Glazer, L., and Shilo, B.Z. (2001). Hedgehog signaling patterns the tracheal branches. Development 128, 1599–1606.

Grün, D., Wang, Y.L., Langenberger, D., Gunsalus, K.C., and Rajewsky, N. (2005). microRNA target predictions across seven Drosophila species and comparison to mammalian targets. PLoS Comput. Biol. 1, e13.

Guillemin, K., Groppe, J., Ducker, K., Treisman, R., Hafen, E., Affolter, M., and Krasnow, M.A. (1996). The pruned gene encodes the Drosophila serum response factor and regulates cytoplasmic outgrowth during terminal branching of the tracheal system. Development 122, 1353–1362.

Hendrickson, D.G., Hogan, D.J., McCullough, H.L., Myers, J.W., Herschlag, D., Ferrell, J.E., and Brown, P.O. (2009). Concordant regulation of translation and mRNA abundance for hundreds of targets of a human microRNA. PLoS Biol. 7, e1000238.

Ingham, P.W., Nakano, Y., and Seger, C. (2011). Mechanisms and functions of Hedgehog signalling across the metazoa. Nat. Rev. Genet. 12, 393–406.

Jiang, J., and Hui, C.C. (2008). Hedgehog signaling in development and cancer. Dev. Cell 15, 801–812.

Jiang, Q., Wang, Y., Hao, Y., Juan, L., Teng, M., Zhang, X., Li, M., Wang, G., and Liu, Y. (2009). miR2Disease: a manually curated database for microRNA deregulation in human disease. Nucleic Acids Res. 37, D98–D104.

Johnson, S.M., Grosshans, H., Shingara, J., Byrom, M., Jarvis, R., Cheng, A., Labourier, E., Reinert, K.L., Brown, D., and Slack, F.J. (2005). RAS is regulated by the let-7 microRNA family. Cell 120, 635–647.

Kayed, H., Kleeff, J., Keleg, S., Guo, J., Ketterer, K., Berberat, P.O., Giese, N., Esposito, I., Giese, T., Büchler, M.W., and Friess, H. (2004). Indian hedgehog signaling pathway: expression and regulation in pancreatic cancer. Int. J. Cancer 110, 668–676.

Krützfeldt, J., and Stoffel, M. (2006). MicroRNAs: a new class of regulatory genes affecting metabolism. Cell Metab. 4, 9–12.

Lal, A., Navarro, F., Maher, C.A., Maliszewski, L.E., Yan, N., O'Day, E., Chowdhury, D., Dykxhoorn, D.M., Tsai, P., Hofmann, O., et al. (2009). miR-24 Inhibits cell proliferation by targeting E2F2, MYC, and other cell-cycle genes via binding to "seedless" 3'UTR microRNA recognition elements. Mol. Cell 35, 610–625.

Lewis, B.P., Shih, I.H., Jones-Rhoades, M.W., Bartel, D.P., and Burge, C.B. (2003). Prediction of mammalian microRNA targets. Cell 115, 787–798.

Li, Y., Wang, F., Lee, J.A., and Gao, F.B. (2006). MicroRNA-9a ensures the precise specification of sensory organ precursors in Drosophila. Genes Dev. 20, 2793–2805.

Li, Y., Zhang, D., Chen, C., Ruan, Z., Li, Y., and Huang, Y. (2012). MicroRNA-212 displays tumor-promoting properties in non-small cell lung cancer cells and targets the hedgehog pathway receptor PTCH1. Mol. Biol. Cell 23, 1423–1434.

Lu, J., Getz, G., Miska, E.A., Alvarez-Saavedra, E., Lamb, J., Peck, D., Sweet-Cordero, A., Ebert, B.L., Mak, R.H., Ferrando, A.A., et al. (2005). MicroRNA expression profiles classify human cancers. Nature 435, 834–838.

Maragkakis, M., Vergoulis, T., Alexiou, P., Reczko, M., Plomaritou, K., Gousis, M., Kourtis, K., Koziris, N., Dalamagas, T., and Hatzigeorgiou, A.G. (2011). DIANA-microT Web server upgrade supports Fly and Worm miRNA target prediction and bibliographic miRNA to disease association. Nucleic Acids Res. 39, W145–W148.

McMahon, A.P., Ingham, P.W., and Tabin, C.J. (2003). Developmental roles and clinical significance of hedgehog signaling. Curr. Top. Dev. Biol. 53, 1–114.

Miska, E.A., Alvarez-Saavedra, E., Abbott, A.L., Lau, N.C., Hellman, A.B., McGonagle, S.M., Bartel, D.P., Ambros, V.R., and Horvitz, H.R. (2007). Most Caenorhabditis elegans microRNAs are individually not essential for development or viability. PLoS Genet. 3, e215.

Paraskevopoulou, M.D., Georgakilas, G., Kostoulas, N., Vlachos, I.S., Vergoulis, T., Reczko, M., Filippidis, C., Dalamagas, T., and Hatzigeorgiou, A.G. (2013). DIANA-microT web server v5.0: service integration into miRNA functional analysis workflows. Nucleic Acids Res. 41, W169–W173.

Poy, M.N., Eliasson, L., Krutzfeldt, J., Kuwajima, S., Ma, X., Macdonald, P.E., Pfeffer, S., Tuschl, T., Rajewsky, N., Rorsman, P., and Stoffel, M. (2004). A pancreatic islet-specific microRNA regulates insulin secretion. Nature 432, 226–230.

Reczko, M., Maragkakis, M., Alexiou, P., Grosse, I., and Hatzigeorgiou, A.G. (2012). Functional microRNA targets in protein coding sequences. Bioinformatics 28, 771–776.

Rehmsmeier, M., Steffen, P., Hochsmann, M., and Giegerich, R. (2004). Fast and effective prediction of microRNA/target duplexes. RNA 10, 1507–1517.

Ruby, J.G., Stark, A., Johnston, W.K., Kellis, M., Bartel, D.P., and Lai, E.C. (2007). Evolution, biogenesis, expression, and target predictions of a substantially expanded set of Drosophila microRNAs. Genome Res. 17, 1850–1864.

Ruiz i Altaba, A. (1999). Gli proteins and Hedgehog signaling: development and cancer. Trends Genet. 15, 418–425.

Samakovlis, C., Hacohen, N., Manning, G., Sutherland, D.C., Guillemin, K., and Krasnow, M.A. (1996a). Development of the Drosophila tracheal system occurs by a series of morphologically distinct but genetically coupled branching events. Development 122, 1395–1407.

Samakovlis, C., Manning, G., Steneberg, P., Hacohen, N., Cantera, R., and Krasnow, M.A. (1996b). Genetic control of epithelial tube fusion during Drosophila tracheal development. Development 122, 3531–3536.

Silver, S.J., Hagen, J.W., Okamura, K., Perrimon, N., and Lai, E.C. (2007). Functional screening identifies miR-315 as a potent activator of Wingless signaling. Proc. Natl. Acad. Sci. USA 104, 18151–18156.

Szuplewski, S., Kugler, J.M., Lim, S.F., Verma, P., Chen, Y.W., and Cohen, S.M. (2012). MicroRNA transgene overexpression complements deficiency-based modifier screens in Drosophila. Genetics 190, 617–626.

Taipale, J., and Beachy, P.A. (2001). The Hedgehog and Wnt signalling pathways in cancer. Nature 411, 349–354.

Varghese, J., Lim, S.F., and Cohen, S.M. (2010). Drosophila miR-14 regulates insulin production and metabolism through its target, sugarbabe. Genes Dev. 24, 2748–2753.

Watkins, D.N., Berman, D.M., Burkholder, S.G., Wang, B., Beachy, P.A., and Baylin, S.B. (2003). Hedgehog signalling within airway epithelial progenitors and in small-cell lung cancer. Nature 422, 313–317.